

Exceptional van Hove Singularities in Pseudogapped Metals

Indranil Paul¹ and Marcello Civelli²

¹Université Paris Cité, CNRS, Laboratoire Matériaux et Phénomènes Quantiques, 75205 Paris, France

²Université Paris-Saclay, CNRS, Laboratoire de Physique des Solides, 91405, Orsay, France

(Dated: September 8, 2023)

Motivated by the pseudogap state of the cuprates, we introduce the concept of an “exceptional” van Hove singularity that appears when strong electron-electron interaction splits an otherwise simply connected Fermi surface into multiply connected pieces. The singularity describes the touching of two pieces of the split Fermi surface. We show that this singularity is proximate to a second order van Hove singularity, which can be accessed by tuning a dispersion parameter. We argue that, in a wide class of cuprates, the end-point of the pseudogap is accessed only by triggering the exceptional van Hove singularity. The resulting Lifshitz transition is characterized by enhanced specific heat and nematic susceptibility, as seen in experiments.

Introduction.— In electronic systems on a lattice, the periodicity of the potential guarantees the existence of saddle points of the dispersion $\epsilon_{\mathbf{k}}$ as a function of the wavevector \mathbf{k} where the velocity $\mathbf{v}_{\mathbf{k}} \equiv \nabla_{\mathbf{k}}\epsilon_{\mathbf{k}}$ vanishes [1, 2]. In two dimensions such van Hove singularities give rise to diverging density of states, which has attracted attention since the early days of condensed matter physics. Since electron-electron interaction is not needed to produce such singularities, they are typically associated with non-interacting physics. The purpose of the current work is to study “exceptional” van Hove singularities, which are saddle points generated by strong electron-electron interaction. As we show below, such a study is particularly useful to understand some unusual properties of several hole-doped cuprates close to the doping where the pseudogap disappears [3–15].

Our main observation is the following. Consider a one-band system whose Fermi surface is simply connected in the weakly interacting limit. Then, the saddle points are necessarily located at high symmetry points in the Brillouin zone where the Fermi surface can open or close. A typical example is the $(\pm\pi, 0)$ and $(0, \pm\pi)$ points for a square lattice when the band extremum is at $(0, 0)$ or (π, π) . This situation is to be contrasted with the case where the interaction is strong enough to induce self-energy corrections that are singular, such as in a pseudogap phase. Then, as shown in Fig. 1(a)-(c), the self energy splits the simply connected Fermi surface into a multiply connected surface (i.e, Fermi pockets, or annular Fermi surfaces), and the saddle point is a result of the touching of two pieces of that surface. In this case the saddle points are not located on high symmetry points, but they lie on high symmetry lines, see arrows in Fig. 1(b), which has important consequences. We describe the resulting interaction driven van Hove singularity as being “exceptional”, to distinguish them from ordinary van Hove singularities that are obtained in the weakly interacting limit.

Model.— The canonical system to illustrate the physics of exceptional van Hove singularities are certain underdoped cuprates in the pseudogap state. Motivated by the

Yang-Rice-Zhang (YRZ) model [16], we describe it by a single band of electrons whose Green’s function is given by

$$G_{\mathbf{k}}(i\omega_n)^{-1} = i\omega_n - \epsilon_{\mathbf{k}} - P_{\mathbf{k}}^2/(i\omega_n - \xi_{\mathbf{k}}). \quad (1)$$

This type of model has been justified through phenomenological [16–20] as well as numerical [21–30] cluster dynamical mean field studies of the strong coupling Hubbard model. An extensive comparison with experiments using the YRZ model has also been reported in Ref. [31]. Here, $\epsilon_{\mathbf{k}} = -2t(\cos k_x + \cos k_y) - 4t' \cos k_x \cos k_y - \mu$

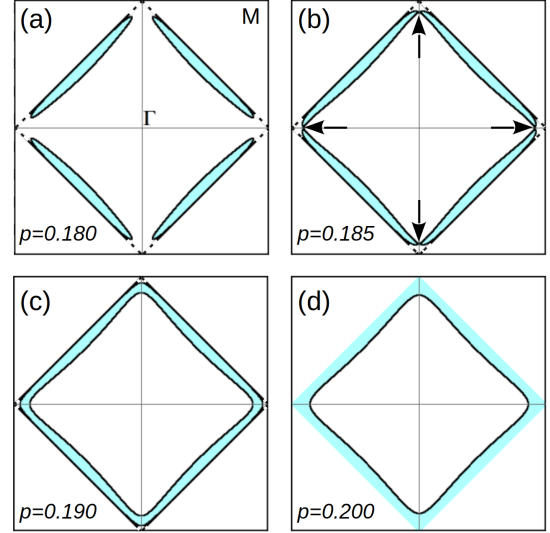


FIG. 1. (Color Online) Fermi surface evolution with doping near the pseudogap end-point. Hole occupation is indicated by blue shade. (a) Singular self energy splits a simply connected Fermi surface into hole pockets. (b) The hole pockets enlarge with doping, and they touch at exceptional van Hove points (indicated by arrows), located on high symmetry lines, but not on high symmetry points. (c) Further doping forms annular rings of holes. (d) When the pseudogap vanishes a closed electron-like weakly interacting Fermi surface is recovered.

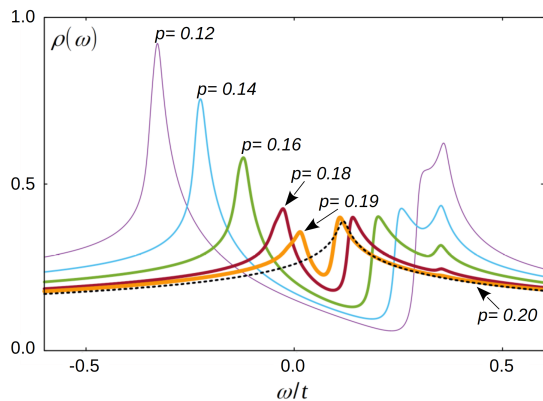


FIG. 2. (Color Online) Density of states $\rho(\omega)$ for various doping. The exceptional van Hove singularity manifests as a peak which is at negative energies ω for low doping. The peak height diminishes as the pseudogap potential decreases with doping. The peak crosses $\omega = 0$ at $p_{ev} \approx 0.185$.

is the electron dispersion, $\tilde{t}(p) = t[1 - 4(0.2 - p)]$ is a hopping parameter modified by the interaction, $t = 1$, $t' = -0.15$, p is the hole doping, and μ is the chemical potential. We take $\xi_{\mathbf{k}} = 2\tilde{t}(\cos k_x + \cos k_y)$, where the equation $\xi_{\mathbf{k}} = -\omega$ defines the points on the Brillouin zone where the electron's spectral weight is suppressed due to the pseudogap. We model the pseudogap by $P_{\mathbf{k}}(p) = \theta(p^* - p)P_0(1 - p/p^*)(\cos k_x - \cos k_y)$, where $\theta(x)$ is the Heaviside step function, $P_0 = 0.4$ is the pseudogap energy at half filling ($p = 0$), and which decreases linearly with hole doping, and terminates at $p^* = 0.2$. All energy scales are in unit of t , which we take to be about 300 meV [32] for later estimates.

Superficially, Eq. (1) is reminiscent of two hybridizing bands, namely the physical electrons with dispersion $\epsilon_{\mathbf{k}}$ and pseudofermions with dispersion $\xi_{\mathbf{k}}$. Thus, it can be written as

$$G_{\mathbf{k}}(i\omega_n) = A_{1\mathbf{k}}/(i\omega_n - \omega_{1\mathbf{k}}) + A_{2\mathbf{k}}/(i\omega_n - \omega_{2\mathbf{k}}), \quad (2)$$

where $\omega_{1\mathbf{k},2\mathbf{k}} = [\epsilon_{\mathbf{k}} + \xi_{\mathbf{k}} \pm \sqrt{(\epsilon_{\mathbf{k}} - \xi_{\mathbf{k}})^2 + 4P_{\mathbf{k}}^2}]/2$. The weight factors $A_{1\mathbf{k}} = (\omega_{1\mathbf{k}} - \xi_{\mathbf{k}})/(\omega_{1\mathbf{k}} - \omega_{2\mathbf{k}})$, and $A_{2\mathbf{k}} = (\xi_{\mathbf{k}} - \omega_{2\mathbf{k}})/(\omega_{1\mathbf{k}} - \omega_{2\mathbf{k}})$. For the doping range studied here only the lower band $\omega_{2\mathbf{k}}$ contributes to the Fermi surface in the form of hole pockets that evolves with doping, see Fig. 1 and Fig. S4 in the Supplementary Information (SI) [33].

Exceptional van Hove singularity.— As shown in Fig. 1, with increasing doping the hole pockets grow and eventually, at a doping $p_{ev} \approx 0.185$, the pockets touch at the van Hove points $(0, \pm k_{ev})$ and $(\pm k_{ev}, 0)$, where $k_{ev} \neq \pi$, see arrows in Fig. 1(b). The resulting Lifshitz transition describes hole pockets merging to form hole rings, see Fig. 1(c).

In the vicinity of such saddle points, say, the one at $(0, k_{ev})$, the dispersion can be expressed as $\omega_{2\mathbf{k}} \approx$

$\alpha k_x^2 - \beta k_y^2 - \gamma k_y k_x^2$, where (α, β, γ) are parameters with dimension of energy, and $\gamma \neq 0$ indicates that the saddle point is not on a high symmetry location. The peak in the density of states $\rho(\omega) \equiv -(1/\pi) \sum_{\mathbf{k}} \text{Im} G_{\mathbf{k}}(\omega + i\Gamma)$ near the singularity is given by $\rho(\omega) \approx 4\rho_{sp}(\omega)$, where

$$\rho_{sp}(\omega) = \frac{1}{2\pi^2 \sqrt{\alpha\beta}} \left[\text{Re} \left[\frac{1}{(1+u)^{1/4}} K(r_1) \right] - \text{Im} \left[\frac{1}{(1+u)^{1/4}} K(r_2) \right] \right]. \quad (3)$$

Here, $u = (\omega + i\Gamma)/E_0$, $E_0 = \alpha^2\beta/\gamma^2$, $r_{1,2}^2 = [1 \pm 1/(1+u)^{1/2}]/2$, and $K(r) \equiv \int_0^{\pi/2} d\theta/\sqrt{1-r^2\sin^2\theta}$ is the complete elliptic integral of the first kind, and $\Gamma = 0.01t$ is a frequency independent inverse lifetime.

In Fig. 2 we show the evolution of the peak in the density of states with doping. As $p \rightarrow p_{ev}$, the peak position moves from negative energies $\omega < 0$, and approaches the chemical potential $\omega = 0$. However, for the cuprates, increasing doping also implies a reduction in the pseudogap strength $P_{\mathbf{k}}(p)$. Therefore, the strength of the singularity decreases upon approaching the Lifshitz transition. This is seen as diminishing peak height of $\rho(\omega)$ with doping in Fig 2.

Proximity to second order van Hove singularity.— This is a consequence of $\gamma \neq 0$. In Fig. 3(a) we plot the curvature $\alpha_{\mathbf{k}} \equiv \partial^2 \omega_{2\mathbf{k}}/\partial k_x^2$ along the $(0, 0) - (0, \pi)$ direction for various doping. We notice that, when the pseudogap is sufficiently small ($p \geq 0.16$), $\alpha_{(0, k_y)}$ has positive values at $k_y \sim 0$, and it has negative values at $k_y \sim \pi$, implying it goes through zero at $k_y = k_2 \sim \alpha/\gamma$.

If $\alpha_{\mathbf{k}} = \mathbf{v}_{\mathbf{k}} = 0$ is simultaneously satisfied, the system has a second order van Hove singularity [37–42]. The density of states has a power law singularity, obtained by taking $\alpha \rightarrow 0$ in Eq.(3), instead of the usual log singularity. In our case these two points are located close by on the same high symmetry lines, i.e. $k_{ev} \sim k_2$, implying that the system is close to the second order singularity, and therefore, the pre-factor of the log is large. Indeed, we find that as $p \rightarrow p^*$, the wavevectors k_{ev} and k_2 come closer, as shown in Fig. 3(b). As shown in Figs. S1 and S2 of the SI [33], the conversion to second order singularity can be readily achieved by varying a third nearest neighbor hopping parameter which, a priori, is feasible in cold atom systems.

Note, for a single band system with a simply connected Fermi surface, no such proximity to a second order van Hove singularity is expected. Thus, in such systems, this proximity distinguishes an interaction induced exceptional van Hove singularity from a weakly interacting ordinary one. In multiband systems, however, higher order van Hove singularities can arise from noninteracting physics alone [37–42].

Exceptional van Hove singularity near pseudogap endpoint.— In the rest of this work we examine the relevance of exceptional van Hove singularities for the cuprates in

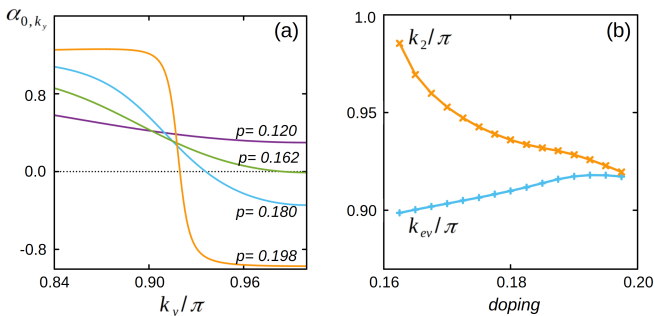


FIG. 3. (Color Online) (a) Plot of $\alpha_{\mathbf{k}} \equiv \partial^2 \omega_{2\mathbf{k}} / \partial k_x^2$ along the $(0,0) - (0,\pi)$ direction for various doping. For $p > 0.162$ in the current model, the curvature $\alpha_{\mathbf{k}}$ vanishes at $(0, k_2)$ and symmetry equivalent points. (b) Variation of k_2 and k_{ev} with doping. Near the pseudogap end-point the exceptional van Hove singularity is close to a second order one, and the prefactor of the log in the density of states is large.

the vicinity of the hole doping p^* where the pseudogap terminates.

First, we explain why, for a large class of cuprates, the chemical potential necessarily crosses the exceptional van Hove singularity as the pseudogap end-point is approached from the underdoped side. As a function of doping (or equivalently, the chemical potential) the evolution of the Fermi surface can be tracked by solving the equation $\text{Re}[G_{\mathbf{k}}(\omega = 0)^{-1}] = 0$. In the absence of any pseudogap term, the self energy corrections are analytic, and therefore the Fermi surface is bound to cross the $(0, \pi)$ and $(\pi, 0)$ points at a doping p_0 where the ordinary (or the weakly interacting) van Hove singularity crosses the chemical potential, thereby transforming from an open to a closed Fermi surface of electrons. In the presence of the pseudogap, however, at $\omega = 0$ the Fermi surface cannot cross these points since the pseudogap term is a divergent repulsive potential on the manifold $\xi_{\mathbf{k}} = 0$ where these points lie. Generally, there are three possible ways in which the Fermi surface evolution can respond to this divergence.

First, the possibility that the pseudogap terminates at a doping exactly where the chemical potential crosses the ordinary van Hove singularity, i.e., $p^* = p_0$. In this case the open Fermi surface can close smoothly by crossing the $(0, \pi)$ and $(\pi, 0)$ points. However, this will occur only if the system is fine-tuned. Since such a coincidence is unlikely in general, we do not discuss it further.

The second possibility is that the pseudogap terminates before the ordinary van Hove singularity is reached, i.e. $p^* < p_0$. In this case, for the doping range $p_0 > p > p^*$, the pseudogap term is zero, the self-energy is analytic, and therefore, the open Fermi surface can close smoothly by crossing the $(0, \pi)$ and $(\pi, 0)$ points. A recent study has shown that this is indeed the case for cuprates for which $|t'/t|$ is sufficiently large, such as $\text{YBa}_2\text{Cu}_3\text{O}_{7-\delta}$

(YBCO), $\text{Tl}_2\text{Ba}_2\text{CuO}_{6+\delta}$, and $\text{HgBa}_2\text{CuO}_{4+\delta}$ [27].

The third possibility, namely $p^* > p_0$ triggers the exceptional van Hove singularity studied here. It is relevant for cuprates for which $|t'/t|$ is sufficiently small, such as $\text{Bi}_2\text{Sr}_2\text{CaCu}_2\text{O}_{8+\delta}$, $(\text{Bi}, \text{Pb})_2(\text{Sr}, \text{La})_2\text{CuO}_{6+\delta}$, $\text{La}_{2-x}\text{Sr}_x\text{CuO}_4$ (LSCO), and (Nd, Eu)-LSCO [27]. In this case, the hole pockets grow with increasing hole doping, but simultaneously the Fermi surface avoids the $(0, \pi)$ and $(\pi, 0)$ points, since $P_{\mathbf{k}} \neq 0$. In such a situation there is invariably a doping p_{ev} , with $p^* > p_{ev} > p_0$, for which the chemical potential crosses the exceptional van Hove singularity and the hole pockets touch at points which lie on the high symmetry lines such as $(0,0) - (0,\pi)$, see Fig. 1(b). Beyond the Lifshitz transition, for $p^* > p > p_{ev}$, the hole pockets merge into a ring of holes with annular Fermi surfaces, see Fig. 1(c). Then, as $p \rightarrow p^*$, the inner Fermi surface of the hole-ring merges with $\epsilon_{\mathbf{k}} = 0$ and the outer Fermi surface of the hole-ring merges with the line of Luttinger zeroes $\xi_{\mathbf{k}} = 0$, see Fig. 1(d).

Therefore, we predict that, in the narrow doping range $p_{ev} < p < p^*$ separating the Lifshitz transition from the pseudogap end-point, the holes form an annular ring bounded by two Fermi surfaces, see Fig. 1(c), with the physical electron weight mostly on the inner Fermi surface. From an angle resolved photoemission perspective this is a state with a closed Fermi surface, but where the $(\pi, 0)$ point is still pseudogapped. Note, this narrow doping range may be difficult to resolve in an experiment. In that case it will appear that the Lifshitz transition and the closing of the pseudogap occur at the same doping, as reported in the recent literature [6–8, 27, 28].

Experimental signatures.— Recently, signatures of unusual thermodynamics have been reported for several cuprates close to the pseudogap endpoint p^* . Thus, the specific heat coefficients $\gamma(T)$ of LSCO, (Nd, Eu)-LSCO, Ca doped YBCO and $\text{Bi}_{2+y}\text{Sr}_{2-x-y}\text{La}_x\text{CuO}_{6+\delta}$ show logarithmic T -dependence [4, 15], while the nematic susceptibility $\chi_{B_{1g}}$ of $\text{Bi}_2\text{Sr}_2\text{CaCu}_2\text{O}_{8+\delta}$ increases considerably in this doping range [5, 6]. Both these observations can be potentially explained by the presence of a nematic quantum critical point (QCP) around p^* , but no such QCP has been identified until now. Moreover, even though an ordinary van Hove singularity can lead to $\gamma(T) \sim \log T$, the observed anomaly was deemed too sharp for such an explanation [4, 15]. As we show below, the above experimental puzzles can be resolved if we assume the presence of an exceptional van Hove singularity, i.e., these systems follow the third possibility discussed above.

We compute the specific heat coefficient $\gamma(T) = C(T)/T$ using

$$C(T) = \int_{-\infty}^{\infty} d\omega \frac{\omega^2/T^2}{\cosh^2[\omega/(2T)]} \rho(\omega),$$

and we show its (p, T) evolution in Fig. 4. As $p \rightarrow p_{ev}$,

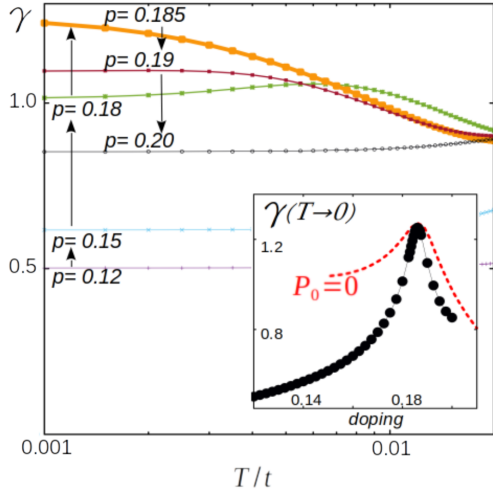


FIG. 4. (Color Online) Specific heat coefficient γ as a function of temperature and doping. Arrows indicate that γ increases as $p \rightarrow p_{ev}$, where the exceptional van Hove singularity is on the chemical potential. At $p = p_{ev}$, the saturation of $\gamma(T)$ with temperature is pushed to lower T . The inset shows the doping dependence of $\gamma(T \rightarrow 0)$ (black dots) with a sharp peak at $p = p_{ev}$. Red dotted line is the calculation for pseudogap $P_{\mathbf{k}} = 0$, and shifted horizontally and vertically for better comparison. The peak is sharper and more pronounced for an exceptional van Hove singularity.

there is a distinct upturn in the T -dependence of the specific heat coefficient, reminiscent of what has been reported for in Refs. [4, 15] with $\gamma(T) \sim \log T$. In our computation there is indeed such a logarithmic component. However, the overall T -dependence in our theory is way more complex, just as is the frequency dependence of the density of states in Eq. (3).

The p dependence of $\gamma(T \rightarrow 0, p)$ is also similar to what has been reported in Refs. [4, 15]. As shown in Fig 4 inset, it has a sharp maxima around $p = p_{ev}$, which is close to, but not coincident with p^* . This sharp feature can be contrasted with the weak coupling case by setting the pseudogap term $P_{\mathbf{k}} = 0$. As shown by the red dotted line in Fig 4 inset, the peak is broader and far less pronounced for an ordinary van Hove singularity compared to an exceptional one. This is because the latter is close to a second order van Hove instability. Also, the bands are flatter than usual for the exceptional case since the velocity vanishes at two proximate points $(0, k_{ev})$ and $(0, \pi)$, instead of only at $(0, \pi)$.

Next, we study the nematic susceptibility in the B_{1g} or the $(x^2 - y^2)$ symmetry channel, which is given by

$$\chi_{B_{1g}} = -\text{Im} \left[\sum_{\mathbf{k}} h_{\mathbf{k}, B_{1g}}^2 \int_{-\infty}^{\infty} \frac{d\omega}{2\pi} \tanh\left[\frac{\omega}{2T}\right] G_{\mathbf{k}}(\omega + i\Gamma)^2 \right],$$

with $h_{\mathbf{k}, B_{1g}} = \partial^2 \epsilon_{\mathbf{k}} / \partial k_x^2 - \partial^2 \epsilon_{\mathbf{k}} / \partial k_y^2$. In Fig. 5 we

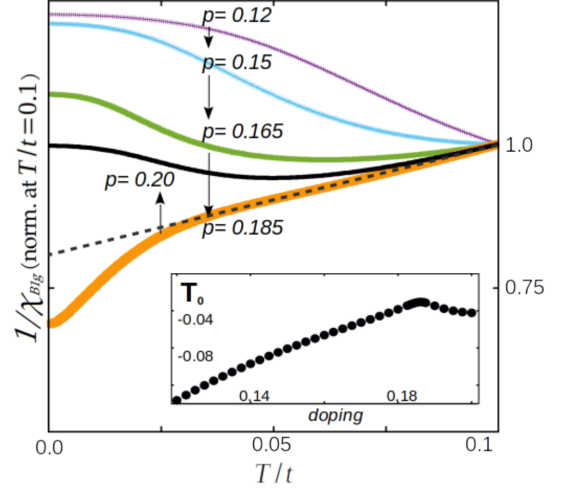


FIG. 5. (Color Online) Temperature and doping dependence of the inverse nematic susceptibility $\chi_{B_{1g}}^{-1}$ in the $(x^2 - y^2)$ channel. The T -dependence enhances considerably around p_{ev} , with Curie-Weiss $1/T$ scaling above a cutoff temperature (black dash line). The inset shows the doping dependence of $T_0 \equiv \chi_{B_{1g}}^{-1}(T \rightarrow 0)$ with a peak near p_{ev} .

present the (p, T) dependencies of $\chi_{B_{1g}}^{-1}$. It has weak T -dependence away from the critical doping p_{ev} , while at p_{ev} it decreases considerably with lowering temperature (equivalently, $\chi_{B_{1g}}(T)$ increases with lowering T), which can be fitted to a Curie-Weiss behavior above a temperature cutoff. Taking $t \sim 300$ meV, the temperature range of the Curie-Weiss behavior in our calculation is 100 K to 300 K, which matches well with the range seen in the experiments. Thus, our result is qualitatively close to what has been reported for $\text{Bi}_2\text{Sr}_2\text{CaCu}_2\text{O}_{8+\delta}$ in Fig. 2(b) of Ref. [5]. Note, the low temperature downturn in $\chi_{B_{1g}}^{-1}$ for $p \sim p_{ev}$ seen in Fig. 5 is a theoretical prediction that can be checked by performing Raman spectroscopy at lower temperatures. Finally, the inset of Fig. 5 shows the doping dependence of $T_0 \equiv \chi_{B_{1g}}^{-1}(T = 0)$. Once again, the non-monotonic p dependence, with T_0 coming close to zero (equivalently, large $\chi_{B_{1g}}$) around $p \sim p_{ev}$, captures what is reported in Fig. 3 of Ref. [5].

Conclusion.— In summary, motivated by the pseudogap state of the cuprates, we introduced the concept of a strong interaction driven “exceptional” van Hove singularity. It appears when the single particle dispersion has a singular correction that splits an otherwise simply connected Fermi surface into multiply connected pieces. The exceptional van Hove singularity describes the touching of two pieces of the split Fermi surface. The associated saddle points of the renormalized dispersion are located, not on high symmetry points, but on high symmetry lines of the Brillouin zone. This feature is proximate to a second order van Hove singularity. Consequently, the loga-

rithmic divergence of the density of states is guaranteed to have a large prefactor. Most importantly, we argued that several hole doped cuprates necessarily encounter an exceptional van Hove point as they approach the pseudogap end point, and we showed that the signatures of the singularity can explain recent experiments [4–6, 15]. We expect the electronic dispersion to show features of the exceptional van Hove which can be detected by photoemission [43, 44] (see discussion associated with Figs. S3 - S5 of the SI for further details [33]).

Finally, our work can be extended in two new directions in the future. First, to study interaction driven second van Hove singularities. Second, to study exceptional van Hove singularities in heavy fermions, where the Kondo coupling with the localized spins provide a singular correction to the conduction electron dispersion.

We are thankful to M. C. O. Aguiar, Y. Gallais, F. Piéchon, A. Sacuto, and L. Taillefer for insightful discussions. We acknowledge financial support from French Agence Nationale de la Recherche (ANR) grant ANR-19-CE30-0019-01 (Neptun).

-
- [1] L. van Hove, *Phys. Rev.* **89**, 1189 (1953).
- [2] see, e.g., N. W. Ashcroft and N. D. Mermin, *Solid State Physics*, Saunders College Publishing, 1976, chapter 8.
- [3] for reviews see, e.g., C. Proust and L. Taillefer, *Annu. Rev. Condens. Matter Phys.* **10**, 409 (2019); I. M. Vishik, *Rep. Prog. Phys.* **81**, 062501 (2018); M. R. Norman, C. Pépin, *Rep. Prog. Phys.* **66**, 1547 (2003).
- [4] B. Michon, C. Girod, S. Badoux, J. Kačmarčík, Q. Ma, M. Dragomir, H. A. Dabkowska, B. D. Gaulin, J.-S. Zhou, S. Pyon, T. Takayama, H. Takagi, S. Verret, N. Doiron-Leyraud, C. Marcenat, L. Taillefer, and T. Klein, *Nature* **567**, 218 (2019).
- [5] N. Auvray, S. Benhabib, M. Cazayous, R. D. Zhong, J. Schneeloch, G. D. Gu, A. Forget, D. Colson, I. Paul, A. Sacuto, and Y. Gallais, *Nat. Comm.* **10**, 5209 (2019).
- [6] S. Benhabib, A. Sacuto, M. Civelli, I. Paul, M. Cazayous, Y. Gallais, M.-A. Méasson, R. D. Zhong, J. Schneeloch, G. D. Gu, D. Colson, and A. Forget, *Phys. Rev. Lett.* **114**, 147001, (2015).
- [7] B. Loret, S. Sakai, S. Benhabib, Y. Gallais, M. Cazayous, M. A. Méasson, R. D. Zhong, J. Schneeloch, G. D. Gu, A. Forget, D. Colson, I. Paul, M. Civelli, and A. Sacuto, *Phys. Rev. B* **96**, 094525 (2017).
- [8] N. Doiron-Leyraud, O. Cyr-Choinière, S. Badoux, A. Ataei, C. Collignon, A. Gourgout, S. Dufour-Beausejour, F. F. Tafti, F. Laliberté, M. Matusiak, D. Graf, M. Kim, J.-S. Zhou, N. Momono, T. Kurosawa, H. Takagi, and L. Taillefer, *Nat. Commun.* **8**, 2044 (2017).
- [9] C. Collignon, A. Ataei, A. Gourgout, S. Badoux, M. Lizaire, A. Legros, S. Licciardello, S. Wiedmann, J.-Q. Yan, J.-S. Zhou, Q. Ma, B. D. Gaulin, N. Doiron-Leyraud, and L. Taillefer, *Phys. Rev. B* **103**, 155102 (2021).
- [10] B. Michon, A. B. Kuzmenko, M. K. Tran, B. McElfresh, S. Komiyama, S. Ono, S. Uchida, and D. van der Marel, *Phys. Rev. Research* **3**, 043125 (2021).
- [11] Y. Fang, G. Grissonnanche, A. Legros, S. Verret, F. Laliberté, C. Collignon, A. Ataei, M. Dion, J. Zhou, D. Graf, M. J. Lawler, P. Goddard, L. Taillefer and B. J. Ramshaw, *Nat. Phys.* **18**, 558 (2022).
- [12] A. Gourgout, G. Grissonnanche, F. Laliberté, A. Ataei, L. Chen, S. Verret, J.-S. Zhou, J. Mravlje, A. Georges, N. Doiron-Leyraud, and L. Taillefer, *Phys. Rev. X* **12**, 011037 (2022).
- [13] M. Zhu, D. J. Voneshen, S. Raymond, O. J. Lipscombe, C. C. Tam, and S. M. Hayden, *Nat. Phys.* **19**, 99 (2023).
- [14] J. Küspert, R. Cohn Wagner, C. Lin, K. von Arx, Q. Wang, K. Kramer, W. R. Pudelko, N. C. Plumb, C. E. Matt, C. G. Fatuzzo, D. Sutter, Y. Sassa, J. -Q. Yan, J. -S. Zhou, J. B. Goodenough, S. Pyon, T. Takayama, H. Takagi, T. Kurosawa, N. Momono, M. Oda, M. Hoesch, C. Cacho, T. K. Kim, M. Horio, and J. Chang, arXiv:2207.07424 [cond-mat.supr-con].
- [15] C. Girod, D. LeBoeuf, A. Demuer, G. Seyfarth, S. Imajo, K. Kindo, Y. Kohama, M. Lizaire, A. Legros, A. Gourgout, H. Takagi, T. Kurosawa, M. Oda, N. Momono, J. Chang, S. Ono, G.-q. Zheng, C. Marcenat, L. Taillefer, and T. Klein, *Phys. Rev. B* **103**, 214506 (2021).
- [16] K.-Y. Yang, T. M. Rice, and F.-C. Zhang, *Phys. Rev. B* **73**, 174501 (2006).
- [17] M. R. Norman, M. Randeria, H. Ding, and J. C. Campuzano, *Phys. Rev. B* **57**, R11093 (1998).
- [18] M. R. Norman, A. Kanigel, M. Randeria, U. Chatterjee, and J. C. Campuzano, *Phys. Rev. B* **76**, 174501 (2007).
- [19] E. Bascones and B. Valenzuela, *Phys. Rev. B* **77**, 024527 (2008).
- [20] J. G. Storey, *EPL* **113**, 27003 (2016).
- [21] B. Kyung, S. S. Kancharla, D. Sénéchal, A.-M. S. Tremblay, M. Civelli, and G. Kotliar, *Phys. Rev. B* **73**, 165114 (2006).
- [22] T. D. Stanescu and G. Kotliar, *Phys. Rev. B* **74**, 125110 (2006).
- [23] A. Liebsch and N.-H. Tong, *Phys. Rev. B* **80**, 165126 (2009).
- [24] M. Civelli, *Phys. Rev. B* **79**, 195113 (2009).
- [25] S. Sakai, Y. Motome, and M. Imada, *Phys. Rev. Lett.* **102**, 056404 (2009).
- [26] S. Sakai, M. Civelli, and M. Imada, *Phys. Rev. Lett.* **116**, 057003 (2016).
- [27] W. Wu, M. S. Scheurer, S. Chatterjee, S. Sachdev, A. Georges, and M. Ferrero, *Phys. Rev. X* **8**, 021048 (2018).
- [28] H. Bragança, S. Sakai, M. C. O. Aguiar, and M. Civelli, *Phys. Rev. Lett.* **120**, 067002 (2018).
- [29] G. Sordi, K. Haule, A.-M.S. Tremblay, *Phys. Rev. Lett.* **104**, 226402 (2010).
- [30] G. Sordi, K. Haule, A.-M. S. Tremblay, *Phys. Rev. B* **84**, 075161 (2011).
- [31] T. M. Rice, K.-Y. Yang, and F. C. Zhang, *Rep. Prog. Phys.* **75** 016502 (2012).
- [32] O. K. Andersen, A. I. Liechtenstein, O. Jepsen, and F. Paulsen, *J. Phys. Chem. Solids* **56**, 1573 (1995).
- [33] See Supplementary Information at [URL will be inserted by publisher] for further details, which also contains Refs. [34–36].
- [34] A. Damascelli, Z. Hussain, and Z.-X. Shen *Rev. Mod. Phys.* **75**, 473 (2003).
- [35] H.-B. Yang, J. D. Rameau, P. D. Johnson, T. Valla, A. Tsvelik, G. D. Gu, *Nature* **456**, 77 (2008).
- [36] M. Zonno, F. Boschini, A. Damascelli, *Journal of Elec-*

- tron Spectroscopy and Related Phenomena **251**, 147091 (2021).
- [37] A. Tamai, M. P. Allan, J. F. Mercure, W. Meevasana, R. Dunkel, D. H. Lu, R. S. Perry, A. P. Mackenzie, D. J. Singh, Z.-X. Shen, and F. Baumberger, Phys. Rev. Lett. **101**, 026407 (2008).
- [38] A. Shtyk, G. Goldstein, and C. Chamon, Phys. Rev. B **95**, 035137 (2017).
- [39] D. V. Efremov, A. Shtyk, A. W. Rost, C. Chamon, A. P. Mackenzie, and J. J. Betouras, Phys. Rev. Lett. **123**, 207202 (2019).
- [40] N. F. Q. Yuan, H. Isobe, and L. Fu, Nat. Comm 10:5769 (2019).
- [41] Y.-T. Hsu, F. Wu, and S. D. Sarma, Phys. Rev. B **104**, 195134 (2021).
- [42] D. Guerci, P. Simon, and C. Mora, Phys. Rev. Res. **4**, L012013 (2022).
- [43] B. Loret, Y. Gallais, M. Cazayous, R. D. Zhong, J. Schneeloch, G. D. Gu, A. Fedorov, T. K. Kim, S. V. Borisenko, and A. Sacuto, Phys. Rev. B **97**, 174521 (2018).
- [44] Y. Zhong, Z. Chen, S.-D. Chen, K.-J. Xu, M. Hashimoto, Y. He, S.-i. Uchida, D. Lu, S.-K. Mo, and Z.-X. Shen, Proc. Natl. Acad. Sci. (USA) **119**, e2204630119 (2022).

Supplementary Information for “Exceptional van Hove Singularities in Pseudogapped Metals”

Indranil Paul¹ and Marcello Civelli²

¹Université Paris Cité, CNRS, Laboratoire Matériaux et Phénomènes Quantiques, 75205 Paris, France

²Université Paris-Saclay, CNRS, Laboratoire de Physique des Solides, 91405, Orsay, France

(Dated: September 8, 2023)

A. Accessing the second order van Hove singularity by tuning a hopping parameter

The purpose of this section is to demonstrate that the exceptional van Hove singularity can be converted into a second order singularity by tuning a hopping parameter. Thus, the logarithmic singularity of the density of states can be fine tuned to a power-law one. Since, in the space of tuning parameters, the exceptional van Hove singularity is close to a second order one, this would imply that, even without fine tuning, the pre-factor of the log in the density of states is typically large.

Accordingly, we consider the same structure of the electronic Green’s function as given by Eq. (1) of the main text, with the bare dispersion now given by $\epsilon_{\mathbf{k}} = -2t(\cos k_x + \cos k_y) - 4t' \cos k_x \cos k_y - 2t''(\cos 2k_x + \cos 2k_y) - \mu$, $t = 1$, $t' = -0.15$, $\mu = -0.885$. We also set the pseudogap scale $P_0 = 0.2$. In other words, we turn on a third nearest neighbor hopping t'' , which is varied in the following. By tuning this parameter the exceptional van Hove singularity becomes a second order one for $t''/t \approx -0.124$. This is shown in Fig. S1. In panel (a) we show the dispersion of the lower band $\omega_{2\mathbf{k}}$, its velocity $\partial\omega_{2\mathbf{k}}/\partial k_y$ and its curvature $\partial^2\omega_{2\mathbf{k}}/\partial k_x^2$ along the high symmetry line $(0, 0)$ to $(0, \pi)$. All the three curves go to zero at the same \mathbf{k} point, indicating that the system

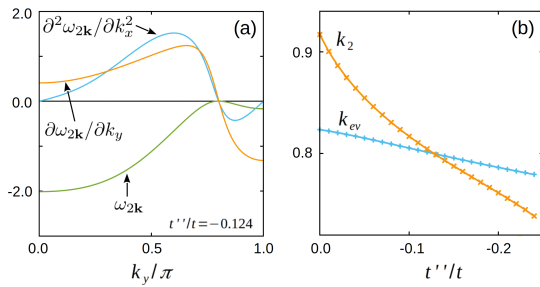


FIG. S1. (Color Online) (a) Plot of the dispersion $\omega_{2\mathbf{k}}$ (green), the velocity $\partial\omega_{2\mathbf{k}}/\partial k_y$ (orange) and the curvature $\partial^2\omega_{2\mathbf{k}}/\partial k_x^2$ (blue) along the high symmetry line $(0, 0)$ to $(0, \pi)$. All the three curves go to zero at the same \mathbf{k} point, indicating that the system is at a second order van Hove singularity. (b) Variations with third nearest neighbor hopping parameter t'' of the points k_{ev} and k_2 , where the velocity $\partial\omega_{2\mathbf{k}}/\partial k_y$ and the curvature $\partial^2\omega_{2\mathbf{k}}/\partial k_x^2$ goes to zero, respectively, along the same high symmetry line. Where they coincide the system is fine tuned to a second order van Hove singularity.

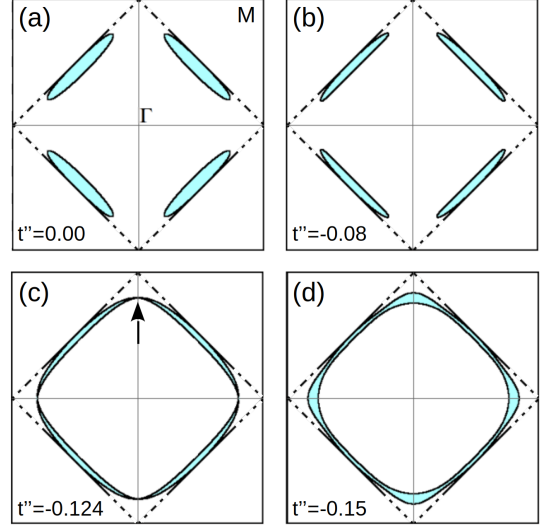


FIG. S2. (Color Online) (a) - (d) Evolution of Fermi surface with the tuning of the third nearest neighbor hopping parameter t'' as the system undergoes a Lifshitz transition in panel (c), where the van Hove point is marked by an arrow. The exceptional van Hove singularity is now of second order as demonstrated in Fig. S1.

is at a second order van Hove singularity. The same can be seen in panel (b) where, as a function of t'' , we track the variation of the points k_{ev} and k_2 , where the velocity $\partial\omega_{2\mathbf{k}}/\partial k_y$ and the curvature $\partial^2\omega_{2\mathbf{k}}/\partial k_x^2$ goes to zero, respectively, along the same high symmetry line. Since the two curves cross, at the fine tuned value of t'' the system has a second order van Hove singularity. Simultaneously, in Fig. S2 we show the evolution of the Fermi surface as the system goes across this singularity.

B. Detection of Exceptional van Hove Singularity by Angle Resolved Photoemission Spectra

We show here that the Lifshitz transition at doping $p = p_{ev}$ associated with the exceptional van Hove singularity (Fig. 1b of the main text) and the appearance of a ring of annular hole Fermi surface for $p_{ev} < p < p^*$ (Fig. 1c of the main text) will have distinct signatures in the band dispersion which can be detected by angle resolved photoemission spectroscopy (ARPES). With this motivation, we display in Fig. S3 the spectral function (see Eq. (2) of the

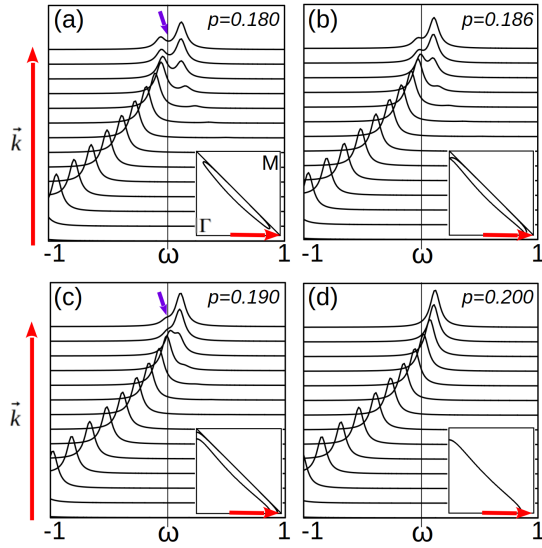


FIG. S3. (Color Online). Spectral peak dispersion of $A(\mathbf{k}, \omega)$ vs ω , accessible by ARPES, plotted along the high symmetry line $(0, 0) \rightarrow (\pi, 0)$, for various doping p across the exceptional van Hove singularity. The x - and y -axes are in unit of t and $1/t$, respectively, where $t \sim 300$ meV.

main text) $A(\mathbf{k}, \omega) = -(1/\pi) \text{Im}G_{\mathbf{k}}(\omega)$, which is directly related to the photoemission spectra, as a function of frequency along the high symmetry \mathbf{k} -line $(0, 0) \rightarrow (\pi, 0)$ of the Brillouin Zone. The exceptional van Hove point $(k_{ev}, 0)$ lies on the chemical potential at the doping p_{ev} along this path, as shown in Fig. 1b of the main text.

When the pseudogap is still sufficiently strong, the Fermi surface forms a hole pocket (see Fig. 1a of the main

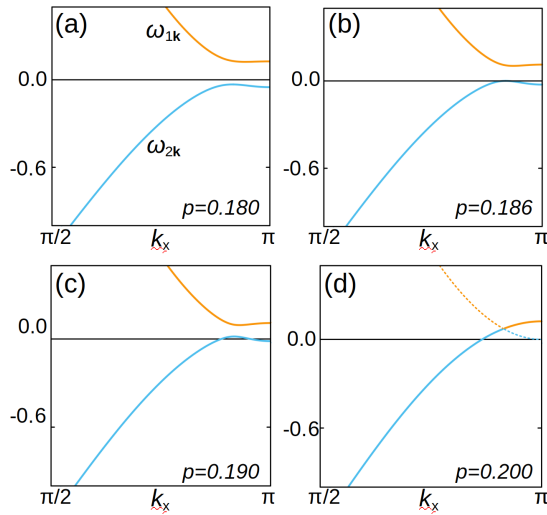


FIG. S4. (Color Online). Band dispersions $\omega_{1\mathbf{k}, 2\mathbf{k}}$ along the high symmetry line $(0, 0) \rightarrow (\pi, 0)$ for various doping p across the exceptional van Hove singularity. Energy is in unit of t .

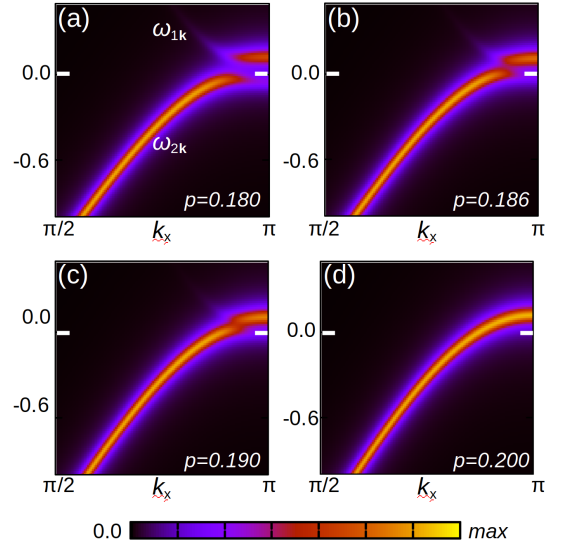


FIG. S5. (Color Online). Spectral intensity plots $A(\mathbf{k}, \omega)$, accessible by ARPES, plotted along the high symmetry line $(0, 0) \rightarrow (\pi, 0)$, for various doping p across the exceptional van Hove singularity. Energy is in unit of t .

text). In Fig. S3.(a) the corresponding spectral function $A(\mathbf{k}, \omega)$ has a peak at $\omega < 0$ which, with increasing k_x , disperses towards the $\omega = 0$ line and then bends back, thereby opening a gap at $(\pi, 0)$. This is the feature that characterizes the pseudogap in ARPES, and it is a well established result (see e.g Ref. [S1]). However, as the doping $p \rightarrow p_{ev}$, this gap closes in the $\omega < 0$ side (Fig. S3.(b)). The peak dispersion tangentially touches the Fermi level at $\omega = 0$ for $k_x = k_{ev}$, and then bends back for increasing k_x . This is the key signature that the exceptional van Hove Lifshitz transition has occurred. Notice that, from the ARPES perspective (which mainly has access to the occupied side $\omega < 0$ of the spectra), this point can be interpreted as the doping p^* where the pseudogap closes. However, according to our results, this doping, rather, marks p_{ev} . Here the pseudogap is small but still present, and is visible in the spectra as a small suppression of the spectral weight just above the Fermi level $\omega > 0$.

By further increasing doping $p_{ev} < p < p^*$, a ring Fermi surface appears (see Fig. 1d of the main text). Therefore we should observe a second Fermi wavevector on the high symmetry line $(0, 0) \rightarrow (\pi, 0)$ and the corresponding quasiparticle peak. However the outer side of the ring is close to the large scattering Yan-Zhang-Rice surface $\xi_{\mathbf{k}} = 0$, which strongly suppresses spectral weight. The quasi-particle peak can be still observed as a shoulder-like feature, which we indicate by the small arrow in Fig. S3(c).

Notice that in this ring Fermi surface region $p_{ev} < p < p^*$, a faint trace of the pseudogap spectral weight suppression is still present in the $\omega > 0$ side. This finally disappears only for or $p \geq p^* = 0.20$, where the more

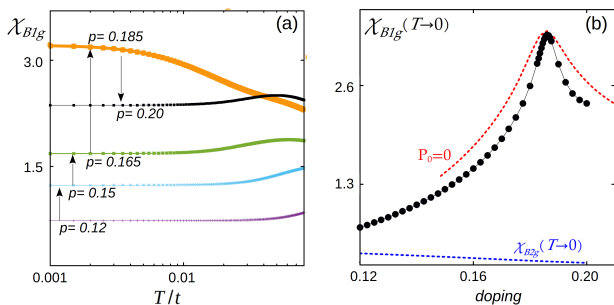


FIG. S6. (Color Online) (a) Temperature and doping dependence of the nematic susceptibility $\chi_{B_{1g}}$ in the $(x^2 - y^2)$ channel. (b) Doping dependence of $\chi_{B_{1g}}(T \rightarrow 0)$ showing a peak near $p \sim p_{ev}$. As in the inset of Fig. 4 of the main text, the peak is sharper and more pronounced compared to an ordinary van Hove singularity (red dotted line). The dashed blue line is the susceptibility $\chi_{B_{2g}}$ in the xy channel, multiplied by a factor 11.1 to allow for a comparison.

typical Fermi liquid peak dispersing through $\omega = 0$ is recovered (Fig. S3d).

These same features, the occurrence of the exceptional van Hove Lifshitz transition and the hole ring Fermi surfaces, could also be observed by looking at the band dispersions $\omega_{1\mathbf{k},2\mathbf{k}}$ (Fig. S4) and the corresponding spectral density plots $A(\mathbf{k},\omega)$ (Fig. S5), which are also accessible by ARPES. These are plotted again along the high symmetry line in momentum space $(0,0) \rightarrow (\pi,0)$. Note, the depth of the hole ring in energy unit, as seen in Fig. S4(c), is of the order of 15 meV, if we take $t \sim 300$ meV. Thus, this feature is within the range of resolution of current ARPES experiments. The $\omega_{1\mathbf{k}}$ in particular shows the contribution from the upper band, which we did not discuss in the main text, as it is not relevant for the exceptional van Hove singularity. It is however crucial to detect the pseudogap closing at p^* . The observation of $\omega_{1\mathbf{k}}$ could allow therefore to definitively distinguish p^* from the exceptional van Hove point p_{ev} . In practice, the full pseudogap could be determined by $\omega_{1\mathbf{k}} - \omega_{2\mathbf{k}}$ in the spectral density plots of Fig. S5. Such a measure within ARPES requires to access the unoccupied states, via thermal excitations for example (as proposed eg in ref. [S2]) or by pump-exciting electrons (as eg in ref. [S3]).

In summary, we show that ARPES spectra can detect the occurrence of an exceptional van Hove Lifshitz transition at a doping $p = p_{ev}$ as a characteristic back-bending of the quasiparticle dispersion. In the doping range $p^* > p > p_{ev}$ we expect to observe a shoulder-like feature in the spectral function $A(\mathbf{k},\omega < 0)$ close to $(\pi,0)$, which indicates the presence of an annular Fermi surface. The persistence of the pseudogap in this doping

range can be also detected if the unoccupied states of the upper band $\omega_{1\mathbf{k}}$ are accessed. That would be a definite proof that $p_{ev} \neq p^*$, and that the Lifshitz transition and pseudogap end point are close but not coincident in the doping axis.

C. Nematic susceptibilities

In Fig. S6(a) we show the temperature and doping dependence of the nematic susceptibility $\chi_{B_{1g}}(T,p)$ on a logarithmic temperature scale. For $p = p_{ev} \approx 0.185$, $\chi_{B_{1g}}(T)$ has considerable temperature dependence, while away from that doping the T -dependence is weak. Likewise, Fig. S6(b) shows that the doping dependence of $\chi_{B_{1g}}(p)$ has a sharp peak around $p \sim p_{ev}$. This is also the behavior seen in doped $\text{Bi}_2\text{Sr}_2\text{CaCu}_2\text{O}_{8+\delta}$. Moreover, above a certain temperature cutoff, $\chi_{B_{1g}}(T)$ at the exceptional van Hove singularity has Curie-Weiss $1/T$ scaling, as reported in the experiments, see Refs. [5, 6] in the main text.

The above can be contrasted with that of $\chi_{B_{2g}}(T,p)$, the nematic susceptibility in the xy symmetry channel, for which the form factor is $h_{\mathbf{k},B_{2g}} = \partial^2 \epsilon_{\mathbf{k}} / \partial k_x \partial k_y$. Since this symmetry channel probes the nodal direction, it is mostly insensitive to the exceptional van Hove singularity, as shown by the dashed blue line in Fig. S6(b). For the sake of completeness we show in Fig. S7 the temperature and doping dependence of $\chi_{B_{2g}}(T)$. Unlike in the case of the B_{1g} response, the B_{2g} response is mostly T -independent, even at p_{ev} . Furthermore, since it is insensitive to the exceptional van Hove point p_{ev} , its behavior as a function of doping is monotonic.

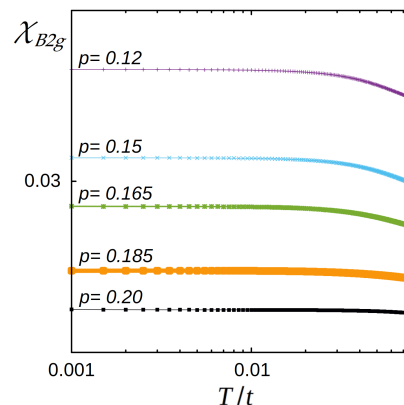


FIG. S7. (Color Online). Temperature dependence of the $\chi_{B_{2g}}(T)$ for various doping p across the exceptional van Hove singularity.

[S1] A. Damascelli, Z. Hussain, and Z.-X. Shen Rev. Mod. Phys. **75**, 473 (2003).

[S2] H.-B. Yang, J. D. Rameau, P. D. Johnson, T. Valla, A.

- Tselik, G. D. Gu, *Nature* **456**, 77 (2008).
- [S3] M. Zonno, F. Boschini, A. Damascelli, *Journal of Electron Spectroscopy and Related Phenomena* **251**, 147091 (2021).